Photoinduced ultrafast transition of the correlated local structure in chalcogenide phase-change materials

Yingpeng Qi[1,3*], Nianke Chen[2], Thomas Vasileiadis[1], Daniela Zahn[1], Hélène Seiler[1], Xianbin Li[2*], Ralph Ernstorfer[1*]

[1]Fritz-Haber-Institut der Max-Planck-Gesellschaft, Faradayweg 4-6, Berlin 14195, Germany

[2]State Key Laboratory of Integrated Optoelectronics, College of Electronic Science and Engineering, Jilin University, 2699 Qianjin Street, Changchun 130012, China

[3]Center for Ultrafast Science and Technology, School of Physics and Astronomy, Shanghai Jiao Tong University, 200240 Shanghai, China

*Correspondence to qiyp@sjtu.edu.cn, lixianbin@jlu.edu.cn and ernstorfer@fhi-berlin.mpg.de

Abstract

Revealing the bonding and time-evolving atomic dynamics in functional materials with complex lattice structures can update the fundamental knowledge on rich physics therein, and also help to manipulate the material properties as desired. As the most prototypical chalcogenide phase change material, $Ge_2Sb_2Te_5$ has been widely used in optical data storage and non-volatile electric memory due to the fast switching speed and the low energy consumption. However, the basic understanding of the structural dynamics on the atomic scale is still not clear. Using femtosecond electron diffraction and TDDFT-MD simulation, we reveal the photoinduced ultrafast transition of the correlated local structure in the averaged rock-salt phase of $Ge_2Sb_2Te_5$. The ultrafast suppression of the local Peierls distortions gives rise to a local structure change from the rhombohedral to the cubic geometry within ~ 0.3 ps.

Our work provides new microscopic insights into contributions of the correlated local structure to the transient structural and optical responses in phase change materials. Moreover, we stress the significance of femtosecond electron diffraction in revealing the correlated local structure in the subunit cell and the link between the correlated disorder and physical properties in functional materials with complex microstructures.

Due to the growth of the global amount of data, the demand for data storage and processing is increasing exponentially [1]. Chalcogenide phase change materials (PCMs) have been singled out as one of the best classes of prospective materials for all-photonic storage/memory [2] and electronic phase-change memory [1]. A laser or electrical pulse stimulates nonvolatile switching between a crystalline and an amorphous phase with atypically large differences in the optical-reflectivity and the electrical-resistivity. Generally, applying a long voltage pulse heats the amorphous phase and leads to recrystallization, and applying a higher voltage pulse to melting and formation of an amorphous phase. Therefore, during such a structural phase switching, the crystallization process is the time-limiting step, while the amorphization process is the energy-intensive step. To optimize these two steps, one hot topic is to modulate the local structural geometry in the atomic level in the most prototypical phase-change material $Ge_2Sb_2Te_5$ (GST-225) and the similar alloys along the tie-line of $GeTe$-Sb_2Te_3 [3-9]. More specifically, the crystallization speed has been improved from tens of nanoseconds to sub-nanosecond by introducing prestructural ordering [4] and crystal precursors [5]. On the other hand, the energy consumption for the amorphization can be reduced by introducing the premelting disordering [6] and controlling the local atomic switching [7]. The recent theoretical studies [8, 9] propose that an ultrafast electronic excitation can also reduce the energy consumption significantly by introducing a direct solid-solid amorphization bypassing the molten state in GST-225. Overall, engineering the local structures in GST-225 and other related phase change materials play a key role in determining and further improving the performance of the structural switching.

The crystalline GST-225 is an averaged rock-salt phase, accompanied by local distortions and huge vacancy concentrations, as shown in Fig. 1a. The anion sub-lattice is fully occupied by Te atoms, whereas the cation sites are populated by Ge (40%), Sb (40%) and vacancies (20%) randomly [3]. The local structure within the unit cell of GST-225 is rhombohedrally distorted with random orientation. Such local distortions with shorter and

longer Ge(Sb)-Te bonds [9, 10, 11] along the [111] direction is termed as local Peierls distortions as shown in Fig. 1a (bottom). From a chemical perspective, the half-filled p-band of Ge (Sb/Te) forms two bonds to the left and right atoms, and this bonding structure is termed resonant bond [12], metavalent bond [13], or multicenter hyperbonding [14]. The randomly oriented Peierls distortions in GST-225 are a typical characteristic of correlated local disorders in crystalline functional materials [15, 16], which can cause intrinsic localized modes [17-20]. The vacancy sites surrounded by Te atoms, as shown in Fig. 1a (bottom), play a crucial role in stabilizing the crystal structure and facilitating the crystal-amorphous transition [11, 21]. Photoexcitation of GST-225 triggers a drastic optical contrast within 100-200 femtoseconds, which has been attributed to the depletion of electrons from the metavalent bonds [22, 23]. Except such an electronic structure modulation, breaking the bond alignment [24] and the medium range order of the lattice structure [25] may also induce a significant change of the optical matrix elements in GST-225. However, the precise knowledge on the ultrafast structural response is still not clear. The initial atomic motions after femtosecond laser excitation have been studied extensively by time-resolved molecular dynamics simulation, ultrafast spectroscopy and ultrafast electron/X-ray diffraction. Nevertheless, the developed structural response models, including the phonon-driven symmetry change [26, 27], the rattling motion [24], the selective bond breaking [8, 9] and the simple thermal response [22, 23], do not provide a consistent picture. Figuring out the transient structural responses will deepen our fundamental understanding of the bonding [12, 13, 21] and the amorphization mechanism [10, 28]. Moreover, for practical applications, identifying the transient atomic motions will benefit the investigation of a direct and energy-efficient amorphization [8, 9].

Ultrafast electron/X-ray probes enable a direct access to transient atomic and electronic motions in a broad range of fundamental physical processes after femtosecond laser excitation, such as the melting [29-31], the chemical reactions [32, 33] and the correlation between subsystems [34, 35]. New phase, which is not accessible in an equilibrium state, can be

created by the photoexcitation-induced change of potential energy surface and the interplay between subsystems [36, 37]. Here we report the photo-induced local structural dynamics in phase change material GST-225 revealed by femtosecond electron diffraction and time-dependent density-functional theory molecular dynamic simulations (TDDFT-MD). The high temporal resolution of ~ 150 fs of our experimental system [38, 39] enables a direct access to the ultrafast structural response beyond a thermal limit. A consistent physical scenario towards an ultrafast transition of the correlated local structure is revealed.
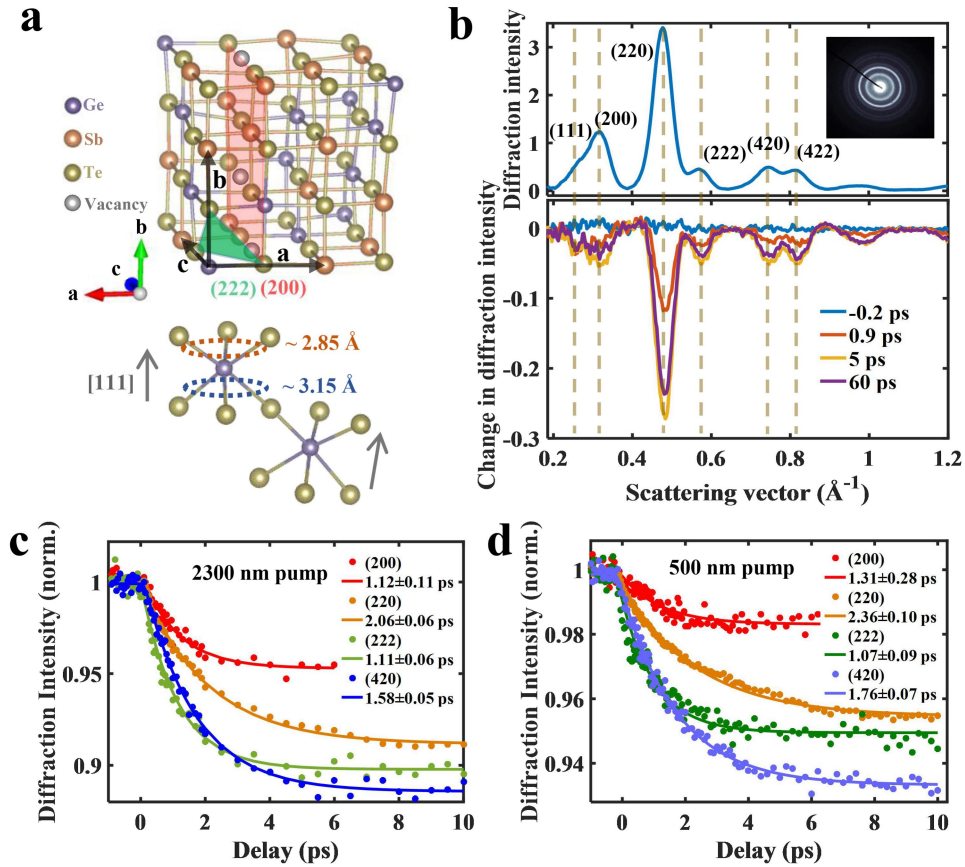
Fig. 1. The crystalline structure and the transient structural dynamics of GST-225. (a) (top) A supercell structure of the rock-salt phase GST-225. The three axes of the unit cell, labeled by a, b and c, are equal in length and the length is 6.01 Å. (bottom) A schematic illustration of randomly oriented Peierls distortions with longer (~ 3.15 Å) and shorter (~ 2.85 Å) Ge(Sb)-Te bonds in the subunit cell. The gray arrows indicate the orientation of the adjacent local rhombohedral structures. (b) (top) The transmission diffraction pattern and the radially averaged intensity distribution (background subtracted) at a negative delay. (bottom) The intensity difference spectrum from -0.2 to 60 ps, calculated by subtracting the intensity distribution at negative delay with 2300 nm and 4.6 mJ/cm^2 laser pump. (c) (left) The temporal evolution of the normalized Bragg reflection intensities with 2300 nm and 4.6 mJ/cm^2 laser pump. The solid lines are the fits with a monoexponential function. (right) The temporal evolution of the normalized Bragg reflection intensities with 500 nm and 0.61 mJ/cm^2 laser pump.

In the experiment, we use a femtosecond laser pulse to excite the GST-225 nanofilm with a thickness of 15 nm (see details in Supplementary Material). A femtosecond electron pulse diffracts off the transient lattice structure at varying time delays. The transmission diffraction pattern and the radially averaged intensity distribution of the rock-salt phase GST-225 are shown in Fig. 1b. Some samples display a partial texture with a preferred (110) orientation, but no impact of such preferred orientation on the transient dynamics was observed through comparing with results from uniform polycrystalline films. The intensity difference spectra in Fig. 1b show a transient decrease of the Bragg reflection intensities after femtosecond laser excitation. To analyze the detailed temporal evolution, we fit an empirical back-ground function (exponential plus second-order polynomial) and pseudo-Voigt line profiles to the peaks in the radial averages at each pump-probe delay [40]. In addition, we double check the time-resolved intensity change and the peak position change by integrating the intensity change and calculating the center-of-mass change respectively over a small area around the maximum of the peak intensity.

Since the band gap of GST-225 is 0.4 ~ 0.5 eV [41], we choose to pump with two different wavelengths, i.e. 2300 nm (0.54 eV) and 500 nm (2.48 eV), in order to investigate the possible impact of the carrier relaxation to the structural response proposed by a recent theoretical study [42]. The relative intensity changes of several Bragg reflections with 2300 nm and 500 nm optical pump are depicted in Fig. 1c and Fig. 1d. We fit the temporal evolution of the intensity with a monoexponential function, convolved with a Gaussian function of 150 fs FWHM to account for the instrument response function. For each reflection, the time constant with 500 nm laser excitation is nearly the same as that with 2300 nm laser excitation, as shown in Fig. 1c and Fig. 1d. With the increase of the pump fluence, the temporal evolution of the intensities and the corresponding time constants are summarized in Fig. S1-S2 and Table 1-2 in Supplementary Material. The observed similar time-resolved intensity change suggests the same structural response with 500 nm and 2300 nm laser

excitation. Whether the carrier relaxation will impact the amorphization process at a higher pump fluence [42] needs to be studied further, but at the low to medium pump fluence, we do not observe any signatures of distinct structural responses after excitation with low photon energy and high photon energy.

The local Peierls distortion is along the <111> direction in the averaged rock-salt phase of GST, therefore, we analyze the (111) reflection in detail in the following. The photo-induced intensity changes of the (111) Bragg reflection are depicted in Fig. 2. To avoid the possible impact of the heat accumulation to the transient structural dynamics [43], experiments at room temperature (Fig. 2a) and at 112 K (Fig. 2b) are performed. The temporal evolution of the intensities and the corresponding intensity difference spectra in Fig. 2a and 2b, clearly indicate an ultrafast intensity decay of the (111) reflection. More information about the raw data and data processing are found in Fig. S3 and S4 in Supplementary Material. The time constant of 0.1 - 0.3 ps for the (111) reflection is significantly smaller than other Bragg reflections in Fig. 1. Given the orientations of the Peierls distortions along the <111> directions, the ultrafast intensity change of the (111) reflection may relate to the local Peierls distortion. Since the Peierls distortion in conventional crystalline material is generally induced by electronic instability, a femtosecond laser excitation will give rise to a suppression of such a structural distortion. For example, in phase change material GeTe, the electronic excitation gives rise to coherent A_{1g} phonon mode and suppresses the long range Peierls distortion [26]. In the case of GST-225, the Peierls distortions are local and randomly oriented along the <111> directions, therefore, the suppression of adjacent local Peierls distortions should be in an incoherent way. The schematic illustration of the suppression of the local Peierls distortion in GST-225 and the corresponding potential energy surface change are shown in Fig. 2c. The photoexcitation flattens the potential energy surface along the [111] direction and enables the opposite movement of the Ge(Sb) and Te atom, giving rise to the local structural transition from the

8

rhombohedral to the cubic geometry. Fig. 2d summarizes the time constant of the intensity

decay of the (111) reflection fitted by a monoexponential function. The overall time constant

at different pump fluences is 0.1 - 0.3 ps, smaller than the period of the A_{1g} phonon mode in
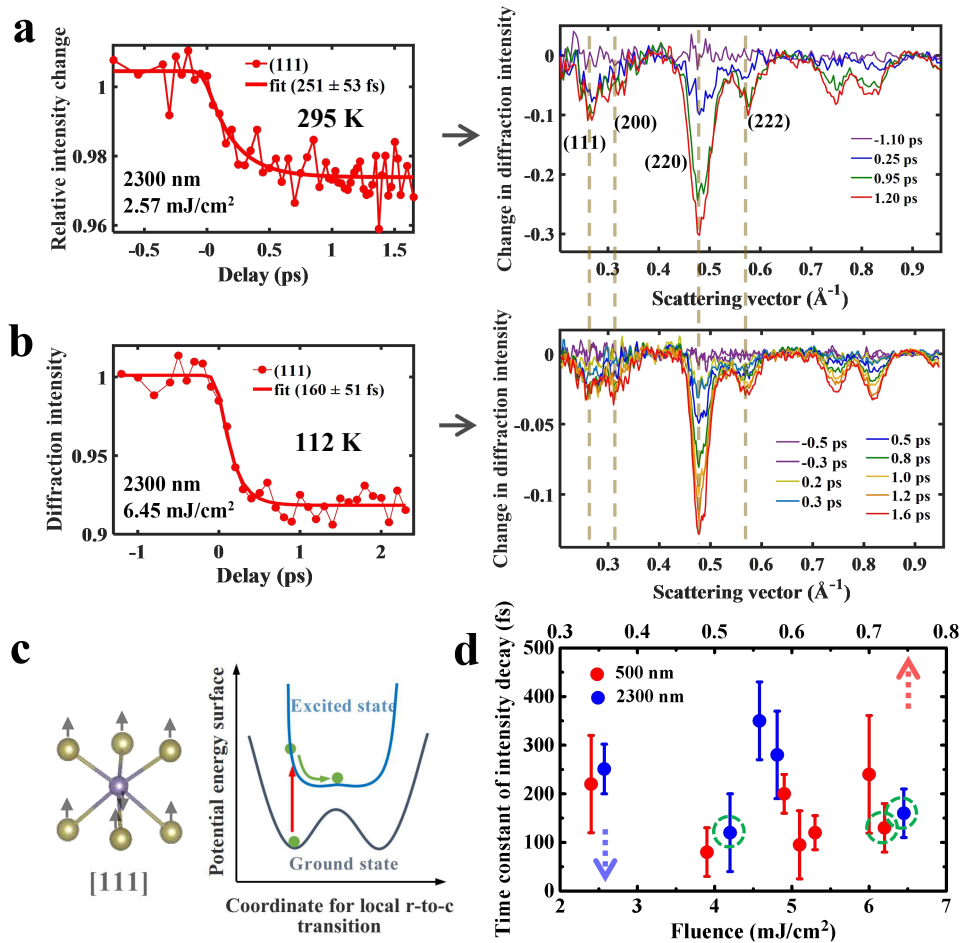
GeTe [26].

Fig. 2. Ultrafast intensity decay of the (111) reflection. (a) (left) Normalized intensity change of the (111) reflection as a function of the time delay with 2300 nm and 2.57 mJ/cm^2 laser pump at room temperature. The solid line is the fit with a monoexponential function. (right) Overall diffraction difference spectrum from -1.10 to 1.20 ps. (b) (left) Normalized intensity change of the (111) reflection as a function of the time delay with 2300 nm and 6.45 mJ/cm^2 laser pump at 112 K. (right) Overall diffraction difference spectrum from -0.5 to 1.6 ps. (c) The schematic illustration of the suppression of the local rhombohedral structure in the subunit cell of rock-salt phase GST-225 and the corresponding potential energy surface change. (d) Changes of the time constant of the (111) reflection depend on the pump fluence and the pump wavelength. The error bars correspond to 68.3% confidence intervals of the fit. The top and the bottom axes are labeled by the fluence of the 500 nm and the 2300 nm laser respectively. The measurements carried out at 112 K are marked with green circles.
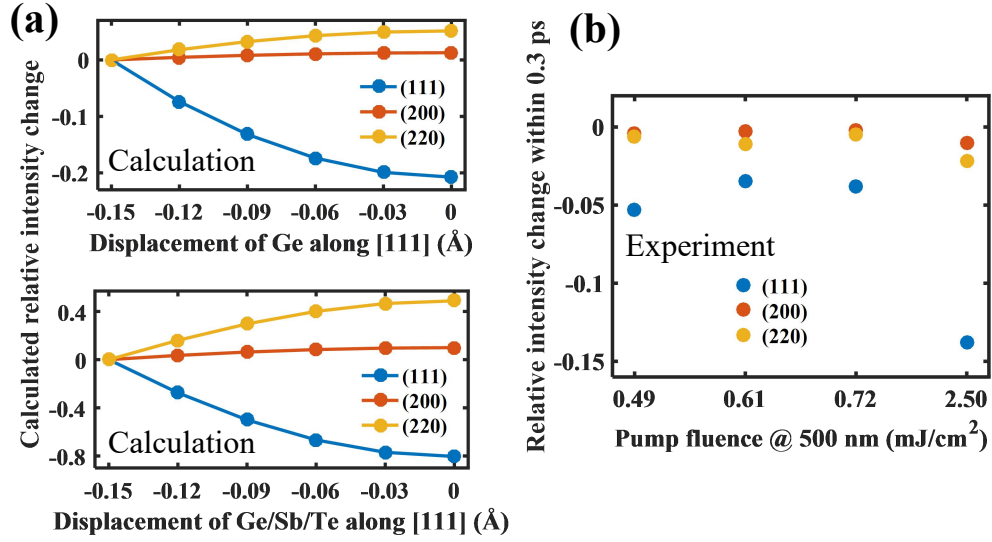
Fig. 3. Calculated and experimental anisotropic intensity change associated with the suppression of the local rhombohedral structure. (a) The relative intensity change of Bragg reflections ($|F|^2$) by structure factor calculation. The zero displacement position indicates the site in an ideal rock-salt phase. The offset displacement of atoms along the [111] direction represents the local rhombohedral structure in one unit cell. In the top figure, only the offset displacement of Ge atom is considered, while in the bottom figure, the opposite displacement of Ge/Sb and Te atom along the [111] direction is used for calculating the intensity change. (b) The measured anisotropic intensity change with 500 nm laser excitation. Within 0.3 ps, the intensity change of the (111) reflection is several times larger than that of (200) and (220) reflection.

To quantify the suppression of the local rhombohedral structure, we perform the structure factor calculation. Note that for crystalline materials with correlated local structure, such as the randomly oriented Peierls distortion in adjacent unit cell in GST-225, the diffraction intensity can be calculated by a summation over all unit cells included. If the atomic motions associated with such local distortions are uncorrelated in different unit cells, the structure factor calculation of a signal unit cell can be used to evaluate the diffraction intensity change of the overall lattice. More detailed information about the structure factor calculation is found in Supplementary Material. The calculation results based on two displacement models are shown in Fig. 3a. It would be reasonable to consider that the lighter Ge atom with larger bond length discrepancy [9] may move more easily while the heavier Te and Sb atoms are rather fixed, therefore, two displacement models are performed. In the first model, only the offset displacement for the Ge atom along the [111] direction is considered, while in the second model, the opposite displacement of Ge/Sb and Te atom along the [111] direction is used for calculating the intensity change. Concomitant with the atomic displacement from the rhombohedral to the cubic configuration (-0.15 Å to 0 Å), the same anisotropic intensity change for the two models is observed, i.e. the intensity of the (111) reflection is decreased significantly while the intensity of the (200) and (220) reflection is enhanced a bit. In Fig. 3b, we extract the experimental intensity change within 0.3 ps. In such an ultrafast timescale, the Debye Waller effect plays a minor role and the intensity change of the (111) reflection just gets finished. As seen, the intensity of the (111) reflection is decreased remarkably while the intensity change for the (200) and (220) reflection is negligible. Such as an anisotropic intensity change is in good agreement with the structure factor calculation in Fig. 3a. The structure factor calculation in Ref. 24 also shows that the movement of locally off-centered Ge (or Sb) atoms toward the center sites gave rise to a significant intensity decrease of the (111) reflection, which is in agreement with our

conclusion of the suppression of the local Peierls distortions. The model of the rattling motion in Ref. 24, based on an experimentally observed unchanged intensity of the (111) reflection, suggests an insistent local rhombohedral structure after femtosecond laser excitation. The signal-to-noise ratio of the intensity change in Ref. 24 is not as good as that in our measurement, which may smear out the intensity change of the (111) reflection and give rise to the rattling model. In contrast to the enhancement of the Peierls distortions with increasing temperature [9], in the laser-excited case we observe an ultrafast reduction of the Peierls distortions. Thus the initial atomic motion after femtosecond laser excitation is identified to be the suppression of the randomly oriented Peierls distortions.
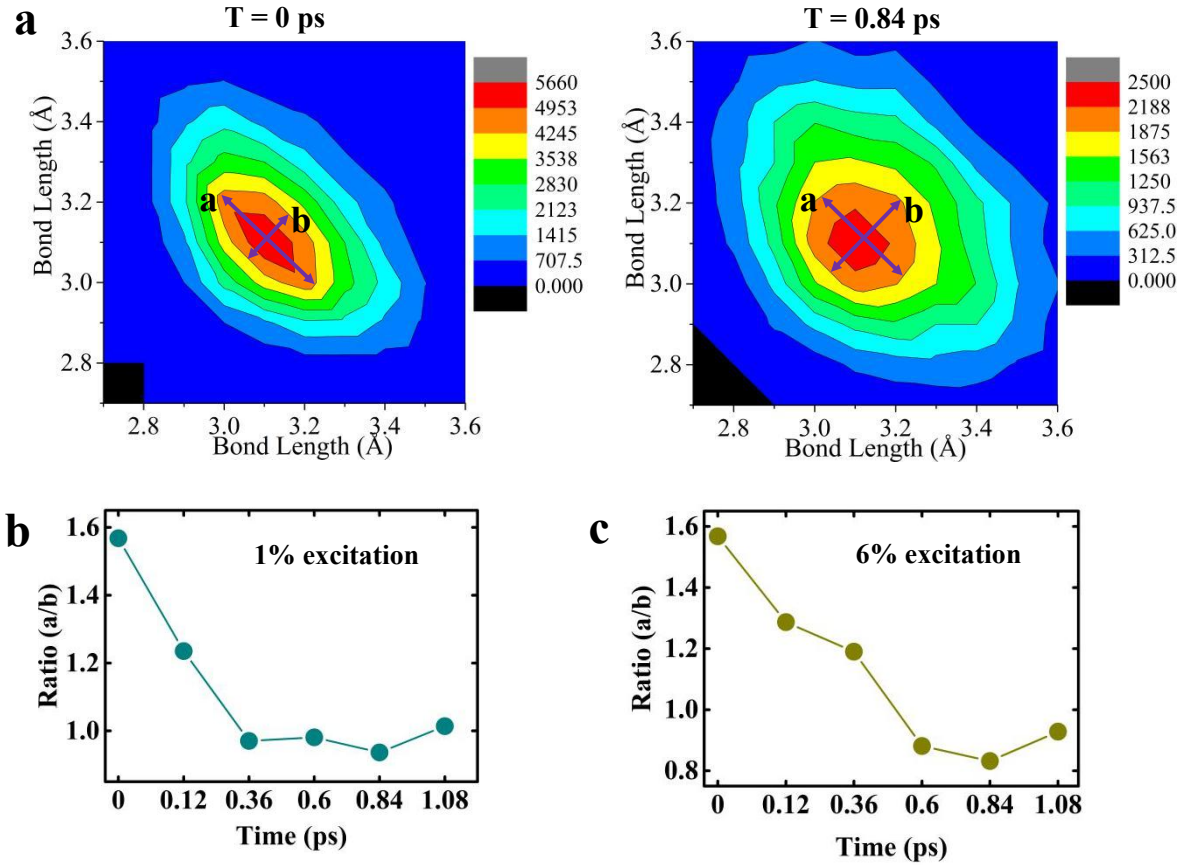
Fig. 4. Simulation results of bond length in linear triatomic bonding geometry in the supercell of GST-225 before and after the electronic excitation. (a) (left) The bond length distribution within the supercell before laser excitation. The tilted distribution indicates a shorter and a longer bond in a linear triatomic bonding geometry. (right) The bond length distribution at 0.84 ps (integration from 0.72 ps to 0.96 ps) after 6% electronic excitation. (b) The temporal evolution of the ratio between the length of line a and line b (indicated in (a)) with 1% electronic excitation. The decrease of the the ratio, i.e. the ellipticity, indicates the suppression of the bond length discrepancy in a linear triatomic bonding geometry. (c) The temporal evolution of ratio between the length of line a and line b with 6% electronic excitation.

We further confirm the photo-induced suppression of local Peierls distortion by performing TDDFT-MD simulations in the averaged rock-salt phase of GST-225. See more detailed information about the simulations in Supplementary Material. The photoexcitation effect is simulated by moving a certain percent of electrons from the valence band maximum states to the conduction band minimum states, similar to the method used in Ref. 26. In order to characterize the bond length discrepancy in the supercell, the bond pairs in each linear triatomic bonding geometry, such as the Te-Ge-Te and the Te-Sb-Te, are tracked during the temporal evolution. The contour map in Fig. 4a displays the distribution of the collected bond pairs. At the ground state (T=0 ps), the elliptical distribution of the contour map in Fig. 4a (left) indicates the shorter and the longer bond in most bond pairs, an intrinsic character of the local Peierls distortions in the averaged rock-salt phase of GST-225. After electronic excitation, as shown in Fig. 4a (right), the ellipticity of the contour map is reduced, i.e. the bond length discrepancy in the bond pair is reduced. In the following, we quantify the change of the bond length discrepancy by calculating the ellipticity of the contour map, i.e. the ratio between the length of line a and line b for the brown zone. The femtosecond laser induced electronic excitation in our experiment is estimated to be a few percent [8], therefore we perform 1% and 6% electronic excitation in the simulation respectively. The temporal evolutions of the ellipticity are displayed in Fig. 4b and Fig. 4c (each data point after electronic excitation is the statistic over the timescale of ± 120 fs). The ellipticity has decreased apparently from 1.6 to around 1, indicating the suppression of the Peierls distortion. Moreover, the change of the ellipticity completes within 0.6 ps, which agrees with the timescale of the ultrafast intensity decay of the (111) reflection in Fig. 2. Therefore, the simulation result coincides with the physical model of the photo-induced reduction of Peierls distortions concluded from the experimental results. The time-

resolved bond length distribution by counting the Te-Ge-Te geometry and the Te-Sb-Te geometry respectively is shown in Fig. S5 in Supplementary Material.

Using femtosecond electron diffraction and TDDFT-MD simulations, we reveal the ultrafast suppression of the local Peierls distortions in the averaged rock-salt phase of GST-225. In contrast to the model of the rattling motion [24], a local structural transition from the rhombohedral to the cubic geometry within ~ 0.6 ps is demonstrated based on the comprehensive study and the high signal-to-noise ratio. Since the Peierls distortion is randomly oriented along different <111> directions, the atomic displacements associated with the suppression of Peierls distortions in adjacent unit cells are incoherent. Therefore, such local structural transition is intrinsically different from the conventional long-range symmetry change, such as the rhombohedral-to-cubic transition in GeTe driven by the coherent A_{1g} phonon mode [26]. The timescale of the ultrafast intensity decay of the (111) reflection in Fig. 2 is comparable to that of the dielectric function change after femtosecond laser excitation [22, 23]. Before the revealing of the ultrafast structural response, the dielectric function change has been solely attributed to the population of the resonant bonds [22, 23]. An interesting question is whether the local structural transition contributes to the giant and ultrafast dielectric function change. Though the bond length discrepancy in the subunit cell is reduced, the incoherent displacements associated with the suppression of local Peierls distortions in adjacent unit cells may induce a more disordered bond angle distribution. In this case, the long-range alignment of the p orbital bonds [12-14] and the vacancy mediated three-center four-electron bonds [14, 21] would break partially, contributing to the dielectric function change.

A direct solid-solid amorphization bypassing the molten state has long been pursued in GST-225 [6-9, 42, 44, 45]. In contrast to the enhancement of the Peierls distortions with rising temperature [9], the identified ultrafast suppression of the local Peierls distortions here is

photo-induced. The similar ultrafast structural responses after excitation with 2300 nm and 500 nm laser pump indicates no significant impact of the carrier relaxation to the structural dynamics, as opposed to predictions from simulations [42]. We expect upon increasing the pump fluence, the suppression of the Peierls distortions will be the intrinsic process driving the system towards the amorphization phase, rather than the model of the selective breaking of the longer bonds in the local distortion [9, 46]. The ultrafast suppression of the local Peierls distortion indicates strong local force and such local force may drive the lattice contraction towards vacancy sites [45, 47]. In this case, a lattice collapse into the amorphous phase, i.e. a direct crystalline to the amorphous phase transition, is possible. Our work indicates that phase change materials with a large bond length discrepancy and a large concentration of vacancies, such as the transition metal embedded phase change materials [5, 48], the phase change heterostructure [49], $GeSb_2Te_4$ [11] and GeSb [50], are interesting platforms to study the underlying direct amorphization by femtosecond laser excitation.

Correlated disorder, such as the randomly oriented Peierls distortions in GST-225 and $BaTiO_3$ (see Ref. 15), is an intrinsic structural character in many functional crystalline materials and is likely important for the particular function of interest [15, 16]. By conventional crystallography technique, only crystal structure with long range order can be detected and the correlated local disorder is invisible. How to characterize the correlated disorder and establish the link between the physical properties and the disorder is challenging. Intrinsically, such correlated disordering by electronic instability may be released in an ultrafast way after femtosecond laser excitation. The corresponding ultrafast atomic motions can be isolated by monitoring the ultrafast intensity changes of specific diffraction peaks as we present in this work. Then the correlated local disorder can be visualized and identified directly with time-resolved diffraction method, such as the ultrafast electron diffraction. We anticipate that the comprehensive analysis of the ultrafast structural responses will help to reveal the correlated disorder [15-20] in crystalline functional materials, and deepen the

understanding of the local structural dynamics in halide perovskites [51, 52] and order-order/disorder structural transitions in thermoelectric materials [53-56] and ferroelectric-paraelectric transitions [57, 58].

Data and materials availability

All data needed to evaluate the conclusions in the paper are present in the paper and the Supplementary Materials. Materials related to this paper may be requested from the corresponding author Yingpeng Qi or Ralph Ernstorfer.

1. W. Zhang, R. Mazzarello, M. Wuttig and E. Ma, Designing crystallization in phase-change materials for universal memory and neuro-inspired computing, *Nat. Rev. Mater*. **4**, 150 (2019).

2. M. Wuttig, H. Bhaskaran and T. Taubner, Phase-change materials for non-volatile photonic applications, *Nat. Photon*. **4**, 83 (2010).

3. M. Wuttig and N. Yamada, Phase-change materials for rewriteable data storage. *Nat. Mater* **6**, 824 (2007).

4. D. Loke, T. H. Lee, W. J. Wang, L. P. Shi, R. Zhao, Y. C. Yeo, T. C. Chong, S. R. Elliott, Breaking the Speed Limits of Phase-Change Memory, *Science* **336**, 1566 (2012).

5. F. Rao et al., Reducing the stochasticity of crystal nucleation to enable subnanosecond memory writing, *Science* **358**, 1423 (2017).

6. Desmond Loke, Jonathan M. Skelton, Wei-Jie Wang, Tae-Hoon Lee, Rong Zhao, Tow-Chong Chong, and Stephen R. Elliott, Ultrafast phase-change logic device driven by melting processes, *Proc. Natl. Acad. Sci.* **111**, 13272 (2014).

7. R. E. Simpson, P. Fons, A. V. Kolobov, T. Fukaya, M. Krbal, T. Yagi and J. Tominaga, Interfacial phase-change memory. *Nat. Nanotech.* **6**, 501 (2011).

8. X. B. Li, X. Q. Liu, X. Liu, D. Han, Z. Zhang, X. D. Han, Hong-Bo Sun, and S. B. Zhang, Role of Electronic Excitation in the Amorphization of Ge-Sb-Te Alloys. *Phys. Rev. Lett.* **107**, 015501 (2011).

9. A. V. Kolobov, M. Krbal, P. Fons, J. Tominaga, and T. Uruga, Distortion-triggered loss of

long-range order in solids with bonding energy hierarchy. *Nat. Chem.* **3,** 311–316 (2011).

10. A. V. Kolobov, P. Fons, A. I. Frenkel, A. L. Ankudinov, J. Tominaga, and T. Uruga, Understanding the phase-change mechanism of rewritable optical media, *Nat. Mater.* **3**, 703 (2004).

11. M. Wuttig, D. Lüsebrink, D. Wamwangi, W. Wełnic, M. Gilleßen, and R. Dronskowski, The role of vacancies and local distortions in the design of new phase-change materials. *Nat. Mater.* 6, 122–128 (2007).

12. K. Shportko, S. Kremers, M. Woda, D. Lencer, J. Robertson and M. Wuttig, Resonant bonding in crystalline phase-change materials, *Nat. Mater.* **7**, 653 (2008).

13. M. Wuttig, V. L. Deringer, X. Gonze, C. Bichara, J. Raty, Incipient Metals: Functional Materials with a Unique Bonding Mechanism, *Adv. Mater.* **30**, 1803777 (2018).

14. T. H. Lee, S. R. Elliott, Chemical Bonding in Chalcogenides: The Concept of Multicenter Hyperbonding, *Adv. Mater.* **32**, 2000340 (2020).

15. A. Simonov and A. L. Goodwin, Designing disorder into crystalline materials, *Nat. Rev. Chem.* **4**, 657 (2020).

16. G. Jeffrey Snyder and Eric S. Toberer, Complex thermoelectric materials, *Nat. Mater.* **7**, 105 (2008).

17. A. J. Sievers, S. Takeno, Intrinsic Localized Modes in Anharmonic Crystals, *Phys. Rev. Lett.* **61**, 970 (1988).

18. D. K. Campbell, S. Flach, Y. S. Kivshar, Localizing energy through nonlinearity and discreteness. *Phys. Today* **57**, 43 (2004).

19. M. E. Manley et al. Intrinsic anharmonic localization in thermoelectric PbSe. *Nat. Commun.* **10**, 1928 (2019).

20. M. E. Manley, A. J. Sievers, J. W. Lynn, S. A. Kiselev, N. I. Agladze, Y. Chen, A. Llobet, and A. Alatas, Intrinsic localized modes observed in the high-temperature vibrational spectrum of NaI, *Phys. Rev. B* **79**, 134304 (2009).

21. A. V. Kolobov, P. Fons, J. Tominaga, and S. R. Ovshinsky, Vacancy-mediated three-center four-electron bonds in GeTe-Sb_2Te_3 phase-change memory alloys. *Phys. Rev. B* **87**, 165206 (2013).

22. L. Waldecker, T. A. Miller, M. Rudé, R. Bertoni, J. Osmond, V. Pruneri, R. E. Simpson, R. Ernstorfer, and S. Wall, Time-domain separation of optical properties from structural transitions in resonantly bonded materials. *Nat. Mater.* **14,** 991–996 (2015).

23. T. A. Miller, M. Rudé, V. Pruneri, and S. Wall, Ultrafast optical response of the amorphous and crystalline states of the phase change material $Ge_2Sb_2Te_5$. *Phys. Rev. B* **94,**

024301 (2016).

24. E. Matsubara *et al.,* Initial Atomic Motion Immediately Following Femtosecond-Laser Excitation in Phase-Change Materials. *Phys. Rev. Lett.* **117***,* 135501 (2016).

25. B. Huang and J. Robertson, Bonding origin of optical contrast in phase-change memory materials, *Phys. Rev. B* **81**, 081204(R) (2010).

26. N. K. Chen, X. B. Li, J. Bang, X. P. Wang, D. Han, D. West, S. B. Zhang, and H. B. Sun, Directional Forces by Momentumless Excitation and Order-to-Order Transition in Peierls-Distorted Solids: The Case of GeTe. *Phys. Rev. Lett.* **120**, 185701 (2018).

27. J. B. Hu, G. M. Vanacore, Z. Yang, X. S. Miao, and A. H. Zewail, Transient Structures and Possible Limits of Data Recording in Phase-Change Materials, *ACS Nano* **97**, 6728-6737 (2015).

28. J. Hegedüs and S. R. Elliott, Microscopic origin of the fast crystallization ability of Ge-Sb-Te phase-change memory materials, *Nat. Mater.* **7**, 399 (2008).

29. D. M. Fritz et al. Ultrafast bond softening in Bismuth: mapping a solid's interatomic potential with X-rays, *Science* **315**, 633 (2007).

30. M. Z. Mo et al. Heterogeneous to homogeneous melting transition visualized with ultrafast electron diffraction, *Science* **360**, 1451 (2018).

31. B. J. Siwick, J. R. Dwyer, R. E. Jordan, R. J. D. Miller, An Atomic-Level View of Melting Using Femtosecond Electron Diffraction, *Science* **302**, 1382 (2003).

32. R. J. Dwayne Miller, Femtosecond Crystallography with Ultrabright Electrons and X-rays: Capturing Chemistry in Action, *Science* **343**, 1108 (2014).

33. Jie Yang et al. Imaging CF_3I conical intersection and photodissociation dynamics with ultrafast electron diffraction, *Science* **361**, 64 (2018).

34. M. Eichberger, H. Schäfer, M. Krumova, M. Beyer, J. Demsar, H. Berger, G. Moriena, G. Sciaini, and R. J. D. Miller, Snapshots of cooperative atomic motions in the optical suppression of charge density waves, *Nature* **468**, 799 (2010).

35. S. Gerber et al. Femtosecond electron-phonon lock-in by photoemission and x-ray free-electron laser, *Science* **357**, 71 (2018).

36. Anshul Kogar et al. Light-induced charge density wave in $LaTe_3$, *Nat. Phys.* **16**, 159 (2020).

37. V. R. Morrison et al. A photoinduced metal-like phase of monoclinic VO_2 revealed by ultrafast electron diffraction, *Science* **346**, 445 (2014).

38. L. Waldecker, R. Bertoni, and R. Ernstorfer, Compact femtosecond electron diffractometer with 100 keV electron bunches approaching the single-electron pulse

duration limit. *J. Appl. Phys.* **117**, 044903 (2015).

39. D. Zahn, P. Hildebrandt, T. Vasileiadis, Y. W. Windsor, Y. Qi, H. Seiler, and R. Ernstorfer, Anisotropic Nonequilibrium Lattice Dynamics of Black Phosphorus. *Nano Lett.* **20**, 3728 (2020).

40. L. Waldecker, R. Bertoni, R. Ernstorfer and J. Vorberger, Electron-Phonon Coupling and Energy Flow in a Simple Metal beyond the Two-Temperature Approximation, *Phys. Rev. X* **6**, 021003 (2016).

41. S. Sahu, A. Manivannan, and U. P. Deshpande, A systematic evolution of optical band gap and local ordering in $Ge_1Sb_2Te_4$ and $Ge_2Sb_2Te_5$ materials revealed by in situ optical spectroscopy, *J. Phys. D: Appl. Phys.* **51** 375104 (2018).

42. J. Bang, Y. Sun, X. Liu, F. Gao, and S. Zhang, Carrier-Multiplication-Induced Structural Change during Ultrafast Carrier Relaxation and Nonthermal Phase Transition in Semiconductors. *Phys. Rev. Lett.* **117,** 126402 (2016).

43. Luciana Vidas, Daniel Schick, Elías Martínez, Daniel Perez-Salinas, Alberto Ramos-Álvarez, Simon Cichy, Sergi Batlle-Porro, Allan S. Johnson, Kent A. Hallman, Richard F. Haglund, Jr., and Simon Wall, Does VO_2 Host a Transient Monoclinic Metallic Phase?, *Phys. Rev. X* **10,** 031047 (2020).

44. P. Fons, H. Osawa, A. V. Kolobov, T. Fukaya, M. Suzuki, T. Uruga, N. Kawamura, H. Tanida, and J. Tominaga, Photoassisted amorphization of the phase-change memory alloy $Ge_2Sb_2Te_5$, *Phys. Rev. B* **82**, 041203(R) (2010).

45. N. K. Chen et al., Giant lattice expansion by quantum stress and universal atomic forces in semiconductors under instant ultrafast laser excitation, *Phys. Chem. Chem. Phys.* **19**, 24735–24741 (2017).

46. K. V. Mitrofanov *et al.,* Sub-nanometre resolution of atomic motion during electronic excitation in phase-change materials. *Sci. Rep.* **6**, 20633 (2016).

47. Z. M. Sun, J. Zhou, Y. C. Pan, Z. Song, H. Mao, and R. Ahuja, Pressure-induced reversible amorphization and an amorphous–amorphous transition in $Ge_2Sb_2Te_5$ phase-change memory material, *Proc. Natl. Acad. Sci.* **108**, 10410 (2011).

48. X. P. Wang, X. B. Li, N. K. Chen, J. Bang, R. Nelson, C. Ertural, R. Dronskowski, H. B. Sun, and S. B. Zhang, Time-dependent density-functional theory molecular-dynamics study on amorphization of Sc-Sb-Te alloy under optical excitation, *Npj Comput. Mater.* **6**, 31 (2020).

49. K. Y. Ding et al., Phase-change heterostructure enables ultralow noise and drift for memory operation, *Science* **366**, 210 (2019).

50. P. Zalden et al. Femtosecond x-ray diffraction reveals a liquid–liquid phase transition in phase-change materials, *Science* **364**, 1062 (2019).

51. J. P. H. Rivett, L. Z. Tan, M. B. Price et al., Long-lived polarization memory in the electronic states of lead-halide perovskites from local structural dynamics. *Nat. Commun.* **9**, 3531 (2018).

52. C. Gehrmann, D. A. Egger, Dynamic shortening of disorder potentials in anharmonic halide perovskites. *Nat. Commun.* **10**, 3141 (2019).

53. E. S. Božin, C. D. Malliakas, P. Souvatzis, T. Proffen, N. A. Spaldin, M. G. Kanatzidis, and S. J. L. Billinge, Entropically Stabilized Local Dipole Formation in Lead Chalcogenides, *Science* **330,** 1660 (2010).

54. T. Keiber, F. Bridges, B. C. Sales, Lead Is Not Off Center in PbTe: The Importance of r - Space Phase Information in Extended X-Ray Absorption Fine Structure Spectroscopy. *Phys. Rev. Lett.* **111***, 095504 (2013).

55. M. P. Jiang et al., The origin of incipient ferroelectricity in lead telluride, *Nat. Commun.* **7**, 12291 (2016).

56. B. Sangiorgio, E. S. Bozin, C. D. Malliakas, M. Fechner, A. Simonov, M. G. Kanatzidis, S. J. L. Billinge, N. A. Spaldin, and T. Weber, Correlated local dipoles in PbTe, *Phys. Rev. Materials* **2**, 085402 (2018).

57. M. Paściak, T. R. Welberry, J. Kulda, S. Leoni, and J. Hlinka, Dynamic Displacement Disorder of Cubic BaTiO$_3$, *Phys. Rev. Lett* **120**, 167601 (2018).

58. K. Datta, I. Margaritescu, D. A. Keen, and B. Mihailova, Stochastic Polarization Instability in PbTiO$_3$, *Phys. Rev. Lett* **121**, 137602 (2018).